Mathematics

Research article

Convective boundary layer flow of MHD tangent hyperbolic nanofluid over stratified sheet with chemical reaction

Reem K. Alhefthi[1], Irum Shahzadi[2], Husna A. Khan[2], Nargis Khan[3], M. S. Hashmi[4,*] and Mustafa Inc[5,*]

[1] Department of Mathematics, College of Sciences, King Saud University, Riyadh 11451, Saudi Arabia
[2] National College of Business Administration and Economics, Bahawalpur, Pakistan
[3] Department of Mathematics, The Islamia University of Bahawalpur, Bahawalpur, Pakistan
[4] Department of Mathematics, The Govt. Sadiq College Women University, Bahawalpur, Pakistan
[5] Department of Mathematics, Firat University, 23119 Elazig, Turkiye

*Correspondence: Email: sadiq.hashmi@gmail.com, minc@firat.edu.tr.

Abstract: We investigated the combined impact of convective boundary conditions, thermal conductivity, and magnetohydrodynamic on the flow of a tangent hyperbolic nanofluid across the stratified surface. Furthermore, the ramifications of Brownian motion, thermophoresis, and activation energy were considered. Heat generation, chemical reactions, mixed convection, thermal conductivity, and other elements were considered when analyzing heat transfer phenomena. The governing equations were converted via similarity transformations into non-dimensional ordinary differential equations in order to analyze the system. Using the shooting method, the problem's solution was determined. We showed the mathematical significance of the temperature, concentration profiles, and velocity of each fluid parameter. These profiles were thoroughly described and shown graphically. The findings demonstrated that as the Weissenberg number and magnetic number increased, the fluid velocity profile decreased. Higher heat generation and thermophoresis parameters resulted in an increase in the temperature profile. Higher Brownian motion and Schmidt parameter values resulted in a drop in the concentration profile. Tables were used to discuss the numerical values of skin friction (C_{fx}), Nusselt number (Nu_x), and Sherwood number (Sh_x). For the greater values of Weissenberg number and mixed convection parameters, skin friction numerical values fell while Nusselt numbers rose.

Nomenclature:

(x, y)	Cartesian coordinate system $[m]$	(u, v)	Velocity field of fluid $[ms^{-1}]$
g	Gravitational acceleration $[ms^{-2}]$	β_T	Thermal expansion coefficient $[K^{-1}]$
v	Kinematic viscosity of the fluid $[m^2 s^{-1}]$	T_∞	Substantial temperature $[K]$
T	Temperature inside boundary $[K]$	C_p	Specific heat of nanoparticle $[Jkg^{-1}k^{-1}]$
T_f	Fluid temperature $[K]$	C_f	Fluid concentration $[kgm^{-3}]$
β_C	Solutal expansion coefficient $[K^{-1}]$	ρ_f	Fluid density $[kgm^{-3}]$
C_∞	Ambient concentration $[kgm^{-3}]$	K_r	Chemical reaction $[mol/L/s]$
β_o	Magnetic field $[kgs^{-2}A^{-1}]$	S	Heat generation/ absorption $[cm^{-1}]$
σ	Fluid Electrical conductivity $[sm^{-1}]$	D_T	Thermophoresis diffusion coefficient $[m^2 s^{-1}]$
D_β	Brownian diffusion coefficient $[m^2 s^{-1}]$	η	Dimensionless similarity variable
$\tilde{n}$	Power index	Γ	Time dependent material constant
M	Magnetic parameter	λ	Parameter of mixed convection
N	Thermal buoyancy forces	Pr	Prandtle number
Nb	Brownian motion parameter	Sc	Schmidt number
Nt	Thermophoresis parameter	We	Weissenberg number
γ	reaction parameter	Gr^*	Grashof number due to concentration
Gr	Grashof number due to temperature	E	Activation energy
δ	Temperature difference		

1. Introduction

Many technical and industrial processes, including food mixing in the gut, blood and plasma flow, the flow of alloys containing mercury, and the lubrication of corrosive oils and greases from the system, use non-Newtonian fluids. Because of numerous technical and industrial uses, many scholars have been interested in the investigation of boundary layer flow and heat transfer in non-Newtonian fluids. Numerous researchers concentrate on non-Newtonian fluid via stretched sheet as the foundation fluid with suspended nanoparticles. Due to this, there has been a lot of interest in studying the thermo-physical properties of non-Newtonian fluids. One of the crucial fluid models among the non-Newtonian fluid is the tangent hyperbolic model. This model makes highly accurate predictions about

the shear thinning phenomena. Additionally, the blood flow is properly characterized by this model. As a result, several constitutive equations of the tangent hyperbolic model are used to describe peristaltic flows.

A nanofluid is containing nanometer-sized particles and conventional base fluid that enhance the combined heat and mass transformed process. Nanofluids are generally specified when nanoparticles are mixed with some base fluids. Nanofluids play a critical role in industrial development in our daily lives such as: in the fields like electronic, automotive, household refrigerators, hybrid drive motors, microelectronics, loops, solar water heater-fuel cells, nuclear power, etc. The first researcher begin to work in this way was Choi [1]. The investigation showed that the addition of nanofluids has significantly increased thermal conductivity. In this respect, Haddad et al. [2] demonstrated a review on natural convective heat transfer of nano fluids. Kalteh et al. [3] discussed a numerical solution of nanofluids with a triangular heat source filled with water-based nanofluid for steady laminar mixed convection flow. The impact of nanoparticle size was explored by Sun 4] who also looked into whether increasing nanoparticle volume improved heat capacity. Shahsavani et al. [5] investigated the non-Newtonian nanofluid flow heat transfer and pressure drop approximation. Shafiq et al. [6–8] worked on an artificial neural network (ANN) to estimate the flow through boundary layer of a nanofluid with convective boundaries. The application of a numerical solution for bioconvective tangent hyperbolic nanofluid flow toward a stretched surface was demonstrated by Shafiq et al. [9,10]. Colak et at. [11] studied the numerical simulation of Darcy-Forchheimer Powell Eyring bioconvective nanofluid flow. Through radiative Riga plate, Shafiq et al. [12] studied the dual stratification on stagnation point Walters' B nanofluid flow.

Many researches do their work using different models of nanofluids. To integrate the properties of thermophoresis and Brownian motion, researchers use the more feasible two phase nanofluid model of Buongiorno. The impacts of thermophoresis and Brownian motion on mass and heat transfer are investigated using Buongiorno's model. This model can be used to calculate the thermophysical properties of nanofluids. These thermophysical properties contribute to the thermal efficiency of several electronic devices. As a result, this model is a useful tool in many engineering fields. Buongiorno's nanofluid model is well suited to the investigation of fluid flow and heat transfer in the different geometries. Mishra and Kumar [13,14] discussed the effect of viscous dissipation and heat generation/absorption on nanofluid flow using the Buongiorno nanofluid model. Khan et al. [15] used Buongiorno model to investigate the non-linear, mixed convective, boundary-driven, tangent hyperbolic nanofluid flow through a cone.

Due to numerous practical uses of MHD, which includes MRI (magnetic resonance imaging) for illness diagnosis, surgical operations, canter action generating hypothermia, and magnetic field effects on wound healing, the investigation of MHD flow is a significant phenomenon. Additionally, the impact of a stretched sheet on the magneto hydrodynamic MHD flow has several uses in contemporary metallurgy and chemical industries, such as cooling nuclear reactors and melting metals. As a result, the scientific community gave MHD fluid flows a lot of attention in the literature. Hayat et al. [16–18] analyze the third-grade fluid's MHD axisymmetric flow over different geometries with heat transfer. Shafiq et al. [19] study the rates of heat, mass and motile microorganisms transfer in the MHD tangent hyperbolic convective flow. Naseem et al. [20] emphasized the behavioral traits of gyrotactic microorganisms to explain mass and heat transport in Powell-Eyring nanofluids when MHD forces are present. Evaluation of mixed convective and chemically reactive nanofluid flow across elongated oblique surfaces when a magnetic field is present is examined by Gupta et al. [21]. Rasool et al. [22]

propose a numerical study of an MHD Williamson nanofluid flow that is kept flowing through a porous medium. Mishra and Kumar [23–25] classify the effects of heat generation/absorption and viscous dissipation into several categories while analyzing the MHD flow of nanofluid across stretched surfaces. The repercussions of MHD in a Darcy-Forchheimer nanofluid flow surrounded by a nonlinearly extending surface are investigated by Rasool et al. [26]. The impact of inclined MHD on a Casson axisymmetric convected nanofluid flow driven by Marangoni is investigated by Shafiq et al. [27] The references [28–30] list a few significant researches on magneto-hydrodynamics (MHD).

In a variety of situations, mixed convection heat-transfer rules can be controlled to maintain temperature rise or fall. Due of their erratic reputation throughout a variety of industries, mixed convective flows have long been of primary interest to scientists and engineers. It performs well in many high-power output devices where forced convection alone does not produce the desired outcome. Convection is being employed now, both naturally occurring and artificially. Nuclear reactor technology and various areas of electronic cooling use the mixed convection principle. There are several instances of mixed convective heat transfer in numerous domains e.g., motorized engineering, thermal organization of electronic devices. Mixed convection heat transfer has recently attained exceptional significance. In an incompressible fluid, Mukhopadhyay et al. [31] investigate how velocity slip and thermal slip affect the mixed convection flow and heat transfer. Imtiaz et al.'s [32] mixed convection flow using nanoparticles is the subject of this study, and we aim to introduce more general convective heat and mass conditions. Haq et al. [33] discussed the purpose of framework to set up the modeling and simulation of mixed convection flow along a water-filled sheet that is being heated vertically. The mixed convection flow of fluid along a stretching sheet was investigated mathematically by Manzzur et al. [34]. Hsiao et al. [35] discussed the subject of mass and heat mixed convection over MHD viscoelastic fluid across a stretching sheet with electromagnetic dissipation. We concentrated on the mass and heat transfer in a continuous laminar boundary-layer flow. Waqas et al. [36] studied the MHD mixed convection flow generated by a micropolar fluid. Ali et al. [37] study the nonlinear convective and radiative flow of a tangent hyperbolic micropolar nanofluid over a magnetized stretching sheet.

Chemically reactive mixes are seen in various circumstances from an industrial perspective, including combustion and chemically designed goods. Seini and Makinde [38] investigate the boundary moved while being affected by radiation and chemical reactions; they found that the boundary layer concentration rose when the reaction rate parameter was raised. According to Sinha [39], examination into the effect of chemical reaction on unsteady free convective flow, enhancing the chemical reaction parameter showed a quicker reaction rate when utilizing a permeable plate and slope temperature. Ali et al. [40–43] investigate the impact of particles aggregation on the thermal conductivity of nanofluid under chemical reaction by the finite element method. Abbas et al. [44,45] investigate the mixed convective and chemically reactive nanofluid flow with Marangoni convection.

In the year 1889, Arrhenius presented the concept of activation energy. For particles to perform a chemical reaction, they require the minimum amount of energy needed. Reactants cannot produce products without this energy, which can be either kinetic or potential. There is a wide range of uses for activation energy, such as in food processing, chemical engineering, geothermal engineering, and oil emulsions. Bestman [46] examined the binary convective amalgam flow over a porous medium in the first part of his investigation. On an intermittent radiated flat porous panel, Makinde et al. [47] investigated the activation energy and effects of the nth-order chemical process. Alsaadi et al. [48] looked into the regressive mixed convective flow of a non-Newtonian nanoliquid across an absorbing

stretched sheet. Abbas et al. [49,50] examined the melting heat transmission and activation energy of different types of nanofluid flow over a slendering stretching sheet.

In light of several real-world issues, heat source/sink influences on heat transport gets huge importance. The addition of a heat sink or source may change the amount of heat distributed throughout the domain. Ramesh et al. [51] investigated the consequences of a non-uniform heat source or sink on mixed convective flow across an inclined stretched surface embedded in an incompressible fluid. Hsiao [52] analyzed the non-uniform heat source/sink with viscoelastic fluid flow throughout a stretching sheet. The fluid flow caused by an asymmetrical heat source/sink has been the subject of numerous studies. The synergistic impact of non-uniform heat source/sink and viscous dissipation on MHD fluid flow was examined by Ramandevi [53]. The influence of a heat source on the Marangoni convective flow of an incompressible hybrid nanofluid with dust particle deferment across a sheet was investigated by Abbas et al. [54].

The literature review cited above reveals that there has been no study on mixed convective boundary layer MHD tangent hyperbolic nanofluid flow over stratified sheet. The current research fills this gap by analyzing the tangent hyperbolic nanofluid flow through a stratified sheet with chemical reaction and activation energy. The novelty of our work is exploring chemical reactions and mixed convection in a MHD tangent hyperbolic nanofluid flow with a Buongiorno nanofluid model, thermal conductivity, activation energy, and heat source. Mixed convection in tangent hyperbolic nano fluid has numerous practical applications in industries where heat transfer is essential. The one application is when heat sinks or heat spreaders are affixed to electronic devices that are attached on a surface to aid in heat transfer. The purpose of the model is to move the nanofluid around the heat-producing elements. The governing PDEs are transformed into dimensionless form utilizing the appropriate similarity transformations. The nonlinear system of ODEs is solved by using the Shooting method (Bilal and Ashbar [55]; Muhammad et al. [56]; Rasheed et al. [57]; Khan et al. [15]). The shooting technique can be computationally efficient, especially when compared to other numerical methods like finite difference or finite element methods. It can handle complex geometries and boundary conditions without excessive computational overhead. It is essential for researching fluid dynamics phenomena in a variety of fields and applications due to its precision and flexibility. The consequences of different physical parameters on the velocity profile, temperature profile, and concentration profile have been discussed by graphs and tables. Tables 1–3 are also used to describe and exhibit the skin friction coefficient, Nusselt, and Sherwood number. The subsequent information revealed our work's distinctiveness even more:

❖ Analyze the behavior of MHD tangent hyperbolic nanofluid flow over a stratified sheet.

❖ In this study, we examine the heat transfer characteristics and two-dimensional tangent hyperbolic nanofluid flow that develop using a convective boundary.

❖ The analysis is carried out while chemical reactions and heat generation/absorption are occurring.

❖ Convective boundary conditions are applied to transfer mass and heat.

❖ Temperature and concentration are the linear functions of diffusivity and thermal conductivity coefficients.

We intend to make theoretical determinations.

❖ Does the coefficient of diffusivity and thermal conductivity affect the flow phenomenon?

❖ What effect does the envisioned tangent hyperbolic nanofluid flow have on the magnetic field?

❖ What influence does the thermal buoyancy parameter have on the velocity profile when nanoparticles are present?

❖ What impact does the Brownian motion and Thermophoresis parameter have on the concentration profile in the presence of nanoparticles?

❖ What impact does the heat absorption and chemical reaction have on the thermal and concentration profiles?

Table 1. Numerical values of $Re_x^{\frac{1}{2}}cf_x$ (skin friction coefficient) for various physical parameters.

n	We	Pr	λ	S	Sc	Nt	Nb	$-Re_x^{\frac{1}{2}}cf_x$
0.2	0.2	1	0.1	0.1	1.5	1.5	0.3	0.83205
0.4								0.70102
0.7								0.32142
0.2	0.1	1	0.1	0.1	1.5	1.5	0.3	0.83637
	0.2							0.83205
	0.5							0.81856
0.2	0.2	2	0.1	0.1	1.5	1.5	0.3	0.83205
		3						0.73059
		4						0.36811
0.2	0.2	1	0.1	0.1	1.5	1.5	0.3	0.83205
			0.2					0.80621
			0.5					0.73355
0.2	0.2	1	0.1	0.1	1.5	1.5	0.3	0.83205
				0.2				0.82862
				0.5				0.81546
0.2	0.2	1	0.1	0.1	0.8	1.5	0.3	0.82836
					1.0			0.82984
					1.5			0.83205
0.2	0.2	1	0.1	0.1	1.5	1.5	0.3	0.83205
						0.5		0.82551
						0.8		0.81915
0.2	0.2	1	0.1	0.1	1.5	1.5	0.3	0.83205
							0.5	0.82907
							0.8	0.82569

Table 2. Numerical values of local Nusselt number $Re_x^{\frac{1}{2}} Nu_x$ for some physical parameters.

E	Pr	λ	M	γ	S	Nt	Nb	$-Re_x^{\frac{1}{2}} Nu_x$
0.1	1	0.1	0.3	1.5	0.1	0.3	0.3	0.24785
0.2			———					0.24781
0.3						———		0.24771
0.2	2	0.1	0.3	1.5	0.1	0.3	0.3	0.26525
	3							0.27146
	4							0.28601
0.2	1	0.1	0.3	1.5	0.1	0.3	0.3	0.26525
		0.2						0.26666
		0.5						0.27009
0.2	1	0.1	0.1	1.5	0.1	0.3	0.3	0.20518
			0.3					0.26525
			0.5					0.30116
0.2	1	0.1	0.3	0.8	0.1	0.3	0.3	0.21942
				1.0				0.23600
				1.5				0.26525
0.2	1	0.1	0.3	1.5	0.1	0.3	0.3	0.26525
					0.2			0.23848
					0.3			0.18583
0.2	1	0.1	0.3	1.5	0.1	0.4	0.3	0.26525
						0.5		0.31532
						0.6		0.38889
0.2	1	0.1	0.3	1.5	0.1	0.3	0.4	0.26525
							0.5	0.26531
							0.6	0.26541

Table 3. Numerical values of Sherwood number $Re_x^{\frac{1}{2}} Sh_x$ for some physical parameters.

E	Pr	λ	M	γ	S	Nt	Nb	$-Re_x^{\frac{1}{2}} Sh_x$
0.1	1	0.1	0.3	1.5	0.1	0.3	0.3	0.16522
0.2			———					0.16532
0.3						———		0.16532
0.2	2	0.1	0.3	1.5	0.1	0.3	0.3	0.26525
	3							0.27146
	4							0.28601
0.2	1	0.1	0.3	1.5	0.1	0.3	0.3	0.26525
		0.2						0.26666

E	Pr	λ	M	γ	S	Nt	Nb	$-Re_x^{\frac{1}{2}}Sh_x$
		0.5						0.27009
0.2	1	0.1	0.1	1.5	0.1	0.3	0.3	0.20518
			0.3					0.26525
			0.5					0.30116
0.2	1	0.1	0.3	0.8	0.1	0.3	0.3	0.21942
				1.0				0.23600
				1.5				0.26525
0.2	1	0.1	0.3	1.5	0.1	0.3	0.3	0.26525
					0.2			0.23848
					0.3			0.18583
0.2	1	0.1	0.3	1.5	0.1	0.4	0.3	0.26525
						0.5		0.31532
						0.6		0.38889
0.2	1	0.1	0.3	1.5	0.1	0.3	0.4	0.26525
							0.5	0.26531
							0.6	0.26541

2. Problem formulation

We investigated the non-Newtonian mixed convection boundary layer hyperbolic tangent nanofluid fluid flow by the stratified sheet that is stable, incompressible, and axisymmetric. The flow is at rest across the surface in the early stages. When x is taken along the wall, the flow is restricted in the domain at $y = 0$, which is in the normal direction to the surface. As shown in Figure 1, a persistent magnetic field is applied in the y-direction. The stratified sheet velocity is assumed to be $u_w(x) = ax$ where 'a' a positive constant. Effects on heat generation and absorption are also taken into account. The boundary conditions for mass and heat convection are used for a stratified sheet.
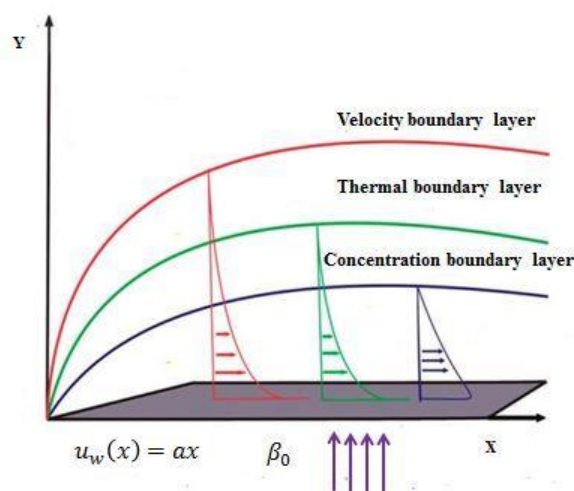
Figure 1. Physical geometry of flow.

The following are the boundary layer equations that regulate the current problem:

Conservation equation of mass (Jawad et al. [58])

$$\frac{\partial u}{\partial x} + \frac{\partial v}{\partial y} = 0. \tag{1}$$

Conservation equation of momentum (Khan et al. [15]):

$$u\frac{\partial u}{\partial x} + v\frac{\partial u}{\partial y} = v(1 - \tilde{n})\frac{\partial^2 u}{\partial y^2} + \sqrt{2}\,\Gamma v \tilde{n}\frac{\partial u}{\partial y}\frac{\partial^2 u}{\partial y^2} - \frac{\sigma\beta_0^2 u}{\rho} + g\beta_T(T - T_\infty) + g\beta_C(C - C_\infty). \tag{2}$$

Energy equation (Khan et al. [15]):

$$u\frac{\partial T}{\partial x} + v\frac{\partial T}{\partial y} = \frac{k}{\rho c_p}\frac{\partial^2 T}{\partial y^2} + \tau\left[D_\beta\left(\frac{\partial c}{\partial y}\frac{\partial T}{\partial y}\right) + \frac{D_T}{T_\infty}\left(\frac{\partial T}{\partial y}\right)^2\right] + \frac{Q}{\rho c_p}(T - T_\infty). \tag{3}$$

Concentration equation (Jawad et al. [58])

$$u\frac{\partial c}{\partial x} + v\frac{\partial c}{\partial y} = D_\beta\frac{\partial^2 c}{\partial y^2} + \frac{D_T}{T_\infty}\frac{\partial^2 T}{\partial y^2} - K_r^2(C - C_\infty)\left(\frac{T}{T_\infty}\right)^n \exp\left(\frac{-Ea}{KT}\right). \tag{4}$$

Having boundary conditions (Khan et al. [15])

$$u = u_w(x) = ax, \; v = 0, \; -k\frac{\partial T}{\partial y} = h_1\left(T_f - T\right), \; D_\beta\frac{\partial c}{\partial y} + \frac{D_T}{T_\infty}\frac{\partial T}{\partial y} = 0 \;\; at \;\; y = 0,$$

$$u \to 0, \; T \to T_\infty, \; C \to C_\infty \quad as \quad y \to \infty. \tag{5}$$

Appropriate transformations for given problem are defined by (Jawad et al. [58])

$$u = xaf'(\eta), \; v = -\sqrt{av}\,f(\eta), \; \eta = y\sqrt{\frac{a}{v}}, \; \theta(\eta) = \frac{T-T_\infty}{T_f-T_\infty}, \; \phi(\eta) = \frac{C-C_\infty}{C_f-C_\infty}. \tag{6}$$

The velocity components in the x - and y -directions are represented by u and v in preceding formulas, Where $v = (\mu/\rho)$ (kinematic viscosity), $\tilde{n}$ (power law index), Γ Williamson parameter), g (gravitational acceleration), β_T (thermal expansion), β_C (concentration expansion), ρ (density), C_ρ (specific heat), k (thermal conductivity), D_β (Brownian diffusion coefficient), D_T (Thermophoresis diffusion coefficient), Q (heat generation/absorption), In the third term of Eq (4) represent the Arrhenius formula in which K_r^2 (rate of reaction), m (dimensionless fitted rate constant), Ea (activation energy) which lies in the range $(-1 < n < 1)$ Ramesh et al. [59]. $u_w(x) = ax$ is the linear stratified sheet velocity. The fluid temperature and concentration are denoted by T and C, while the convective fluid temperature and concentration are denoted by T_f and C_f. The above transformations in Eq (6) are applied to Eqs (2)–(4), and the transformed ordinary differential equations are given as below:

$$(1 - \tilde{n})f''' - (f')^2 + ff'' + \tilde{n}We f'''f'' - Mf' + \lambda(\theta + N\phi) = 0. \tag{7}$$

$$\theta'' + P_r\left(f\theta' + Nb\phi'\theta' + Nt\theta'^2 + S\theta\right) = 0. \tag{8}$$

$$\phi'' + Scf\phi' + \frac{Nt}{Nb}\theta'' - Sc\gamma(1 + \delta\theta)^n \exp\left(\frac{-E}{1+\delta\theta}\right)\phi = 0. \tag{9}$$

The boundary conditions are as follows:

$$f(\eta) = 0, \; f'(\eta) = 1, \; \theta'(0) = -\alpha\big(1 - \theta(0)\big), \; \phi'(0) = -\beta\big(1 - \phi(0)\big) \quad \text{at } \eta = 0,$$

$$\theta(\eta) = 0, \; \phi(\eta) = 0 \quad \text{as } \eta \to \infty, \tag{10}$$

where $\tilde{n}$ is (Power law index) We is (Weissenberg number), λ is (mixed convection), N (ratio of concentration to thermal buoyancy forces), Pr (Prandtle number), Nb (Brownian motion parameter), Nt (Thermophoresis parameter), (heat generation/absorption) S, (Schmidt number) Sc, (reaction rate) γ, (temperature difference) δ, (activation energy) E, Biot numbers α and β, Gr (Grashof number) due to temperature and Gr^* (Grashof number) due to concentration. The temperature at a substantial distance from the wall is shown by T_∞.

These parameters are specified as follows:

$$We = \frac{\sqrt{2a^3}x\Gamma}{\sqrt{v}}, \; \lambda = \frac{Gr}{Re_x^2}, \; N = \frac{Gr^*}{Gr} = \frac{\beta_c(c_f - c_\infty)}{\beta_T(T_f - T_\infty)}, \; Pr = \frac{\mu c_p}{k}, \; Gr = \frac{g\beta_T(T_f - T_\infty)x^3}{v^2}, \; Gr^* = \frac{g\beta_c(C_f - C_\infty)x^3}{v^2},$$

$$S = \frac{Q_0}{a\rho c_p}, Sc = \frac{v}{D_B}, \; Nb = \frac{\tau D_B(C_f - C_\infty)}{v}, \; Nt = \frac{\tau D_T(T_f - T_\infty)}{v T_\infty}, \; \gamma = \frac{K_r^2}{a}, \; \delta = \frac{T_f - T_\infty}{T_\infty}, \; E = \frac{Ea}{KT_\infty}. \tag{11}$$

After using the scaling variables, local skin friction coefficient C_{fx}, Nusselt number Nu_x and Sherwood number Sh_x transform into

$$R_{ex}^{1/2} C_{fx} = 2(1 - \tilde{n})f''(0) - \tilde{n}We f''^3(0),$$

$$Nu_x R_{ex}^{-1/2} = -\theta'(0), \; Sh_x = -\phi'(0), \tag{12}$$

where $R_{ex} = \frac{U_w(x)}{v}$ is local Reynolds number.

3. Graphical results and discussions

The shooting approach is used to find the solution of the modeled equations. As displayed graphically in Figures 2–11, the following section shows the graphical effects of several dimensionless factors on the concentration, temperature, and velocity profiles. Numerous dimensionless parameters $\tilde{n}, \; We, \; M, \; \lambda, \; N, \; Pr, \; Nb, \; Nt, \; S, \; Sc, \; \gamma, \; \delta, \; E,$ and n affect the velocity, temperature, and concentration distributions. The effective parameter range of values has been chosen by following Khan et al. [15], Hayat et al. [60], and Jawad et al. [58], i.e., $0.1 \leq \tilde{n} \leq 0.6, \; 0.1 \leq We \leq 1.5, \; 0.1 \leq M \leq 1.5, \; 0.1 \leq \lambda \leq 0.9, \; 0.1 \leq N \leq 1.5, \; 1.0 \leq Pr \leq 4.0, 0.1 \leq Nb \leq 0.8, \; 0.1 \leq Nt \leq 0.8, 0.1 \leq S \leq 0.7, 0.0 \leq Sc \leq 0.6, \; 0.0 \leq \gamma \leq 0.6, \; 0.1 \leq \delta \leq 0.9, \; 0.2 \leq E \leq 4.0, \; 0.1 \leq n \leq 3.0.$

a) Velocity profile

The impact of $\tilde{n}$ power law index on $f'(\eta)$ velocity is seen in Figure 2(a). It is unambiguous that raising the index power law $\tilde{n}$ lowers the velocity profile. The results show that the fluid nature evolves from shear thinning to shear thickening when power law index $\tilde{n}$ grows. Figure 2(b) shows the effect of We on $f'(\eta)$. It has been perceived that $f'(\eta)$ decreases as the Weissenberg number increases. We Weissenberg number directly correlates with relaxation time i.e., when Weissenberg

We is higher, more resistance is provided and relaxation time rises. Figure 3(a) exhibits impact of M magnetic parameter on the velocity profile. As the magnetic parameter M and the Lorentz force are related, for big magnetic parameter M values, the Lorentz force grows stronger and offers significant resistance to motion, causing the velocity profile to fall. Figure 3(b) shows the impact of λ on the velocity profile. The buoyancy forces are directly related to the mixed convection parameter λ. As a result, the flow's axial velocity changes in response to changes in the mixed convection parameter. Thus, according to theory, a change in the mixed convection leads to an improvement in velocity field. Figure 4(a) depicts the special effects of N on the velocity profile for keeping other parameters fixed. It shows that when the value of N increases it improves the velocity $f'(\eta)$.
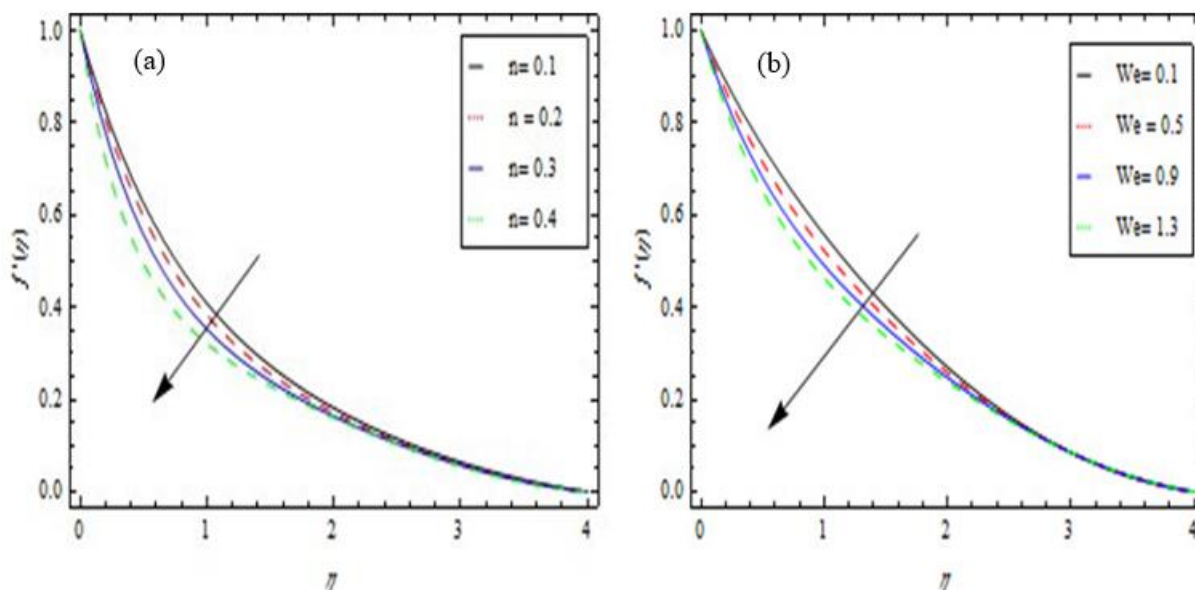
Figure 2. (a) Impact of $\tilde{n}$ on $f'(\eta)$, (b) impact of We on $f'(\eta)$.
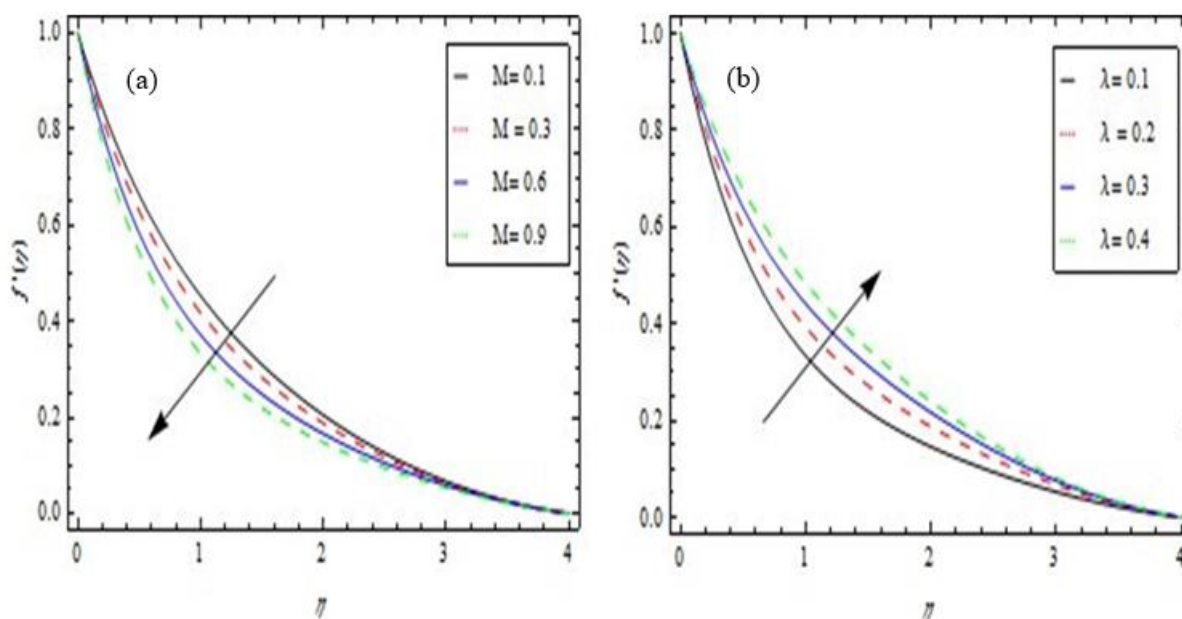
**Figure 3.** (a) Impact of M on $f'(\eta)$, and (b) impact of λ on $f'(\eta)$.
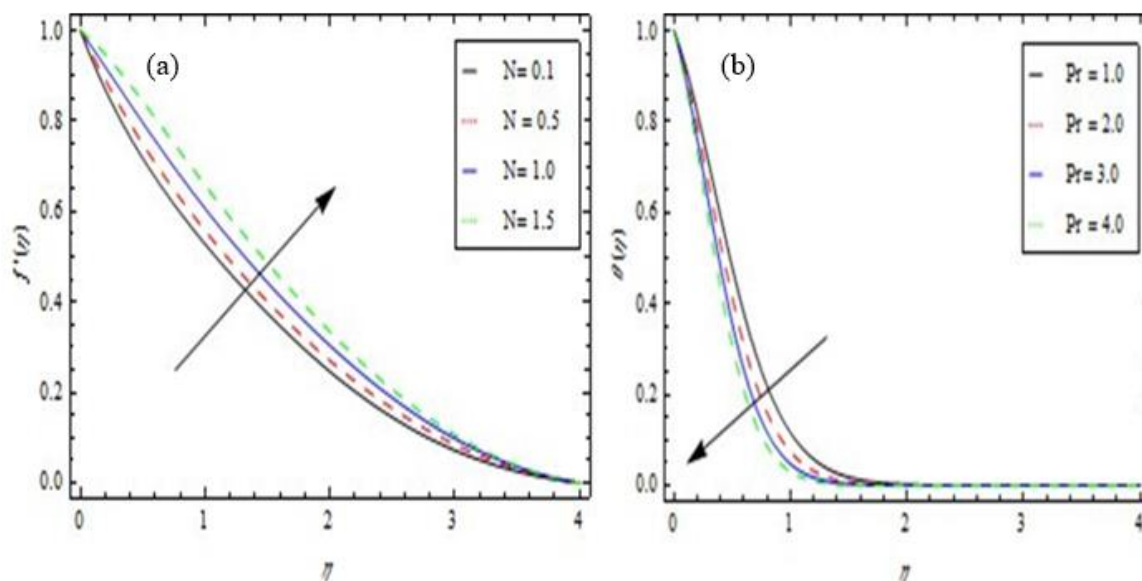
Figure 4. (a) Impact of N on $f'^{(\xi)}$, and (b) Influence of Pr on $\theta(\xi)$.

b) Temperature profile

Figure 4(b) elaborates on the temperature profile variations in relation to Prandtl number Pr. Since thermal conductivity reduces with increasing Prandtl numbers, the temperatures fall down. According to Figure 5(a), the temperature profile $\theta(\eta)$ exhibits an identical pattern when compared to the Brownian motion parameter Nb. Intensification in the Nb Brownian motion parameter causes random motion to move more quickly, which raises the temperature. The consequence of the Nt on temperature is seen in Figure 5(b). It has been demonstrated that the temperature profile raises for high thermophoresis parameter Nt values. A rise in temperature parameter Nt causes the fluid to go from a hot to cold climate. The temperature profile is influenced by the heat generation parameter S, as illustrated in Figure 6(a). The temperature of the flow field is a decreasing function, while its thermal boundary thickness is a rising function of S.
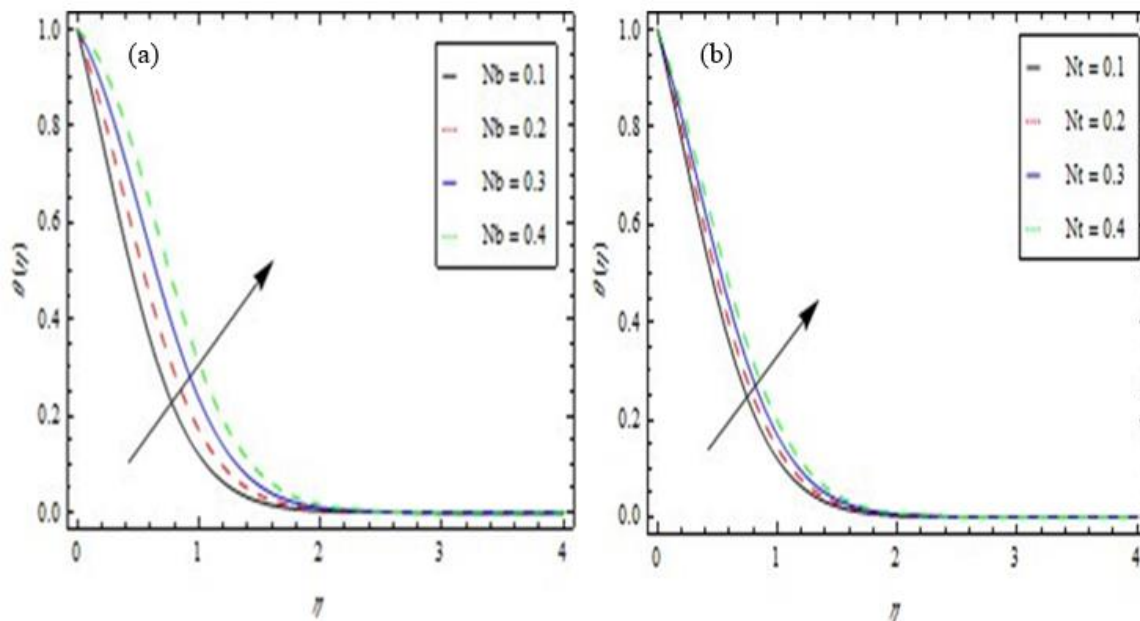
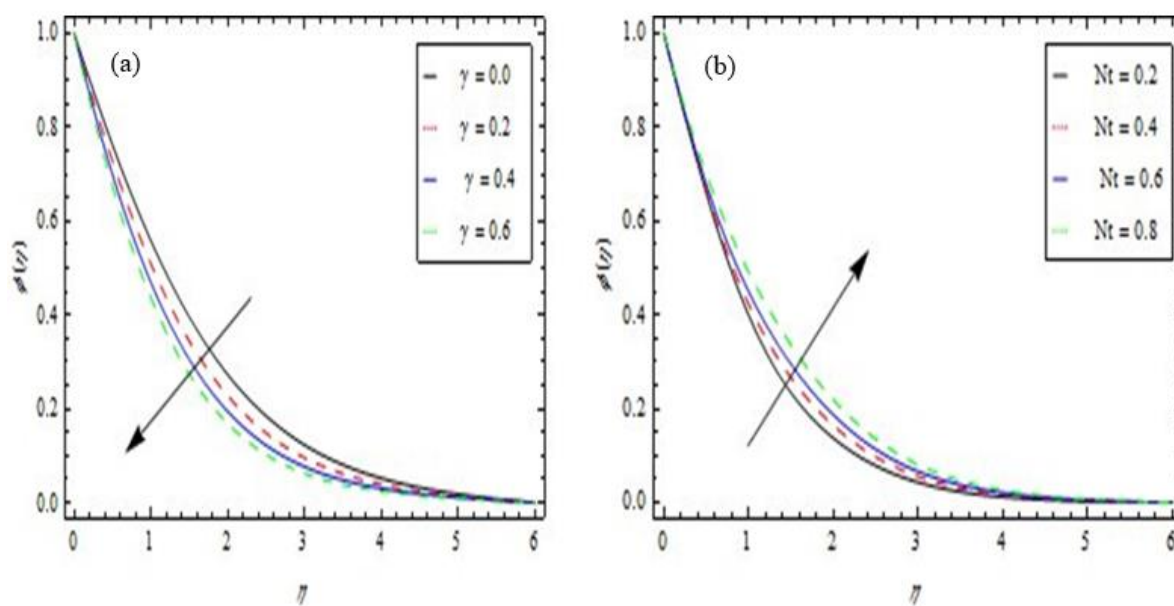**Figure 5.** (a) Influence of Nb on θ(ξ), (b) Influence of Nt on $\theta(\xi)$.
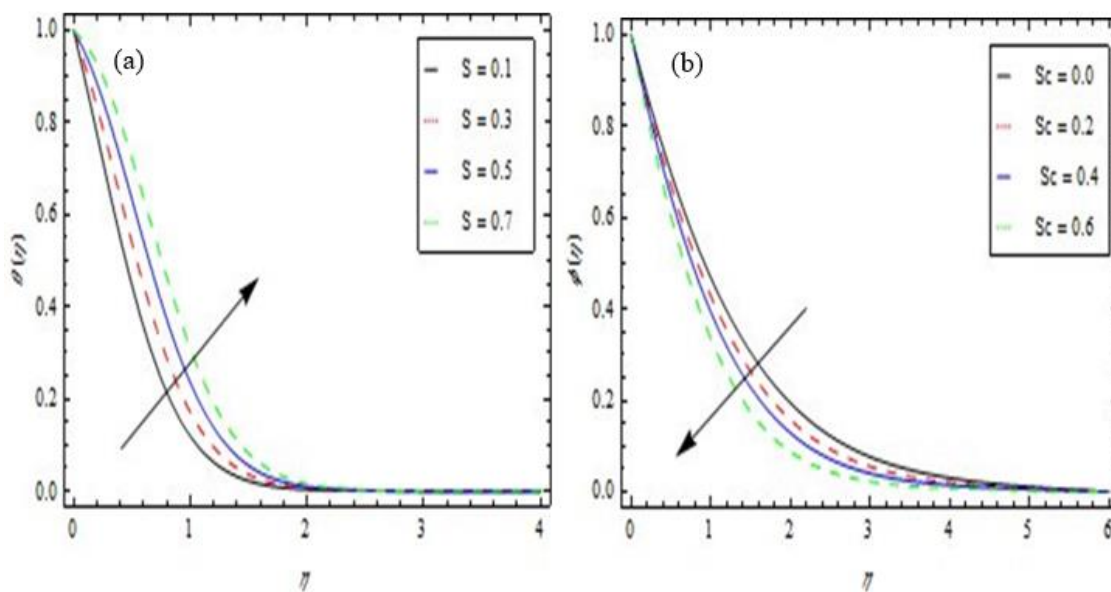
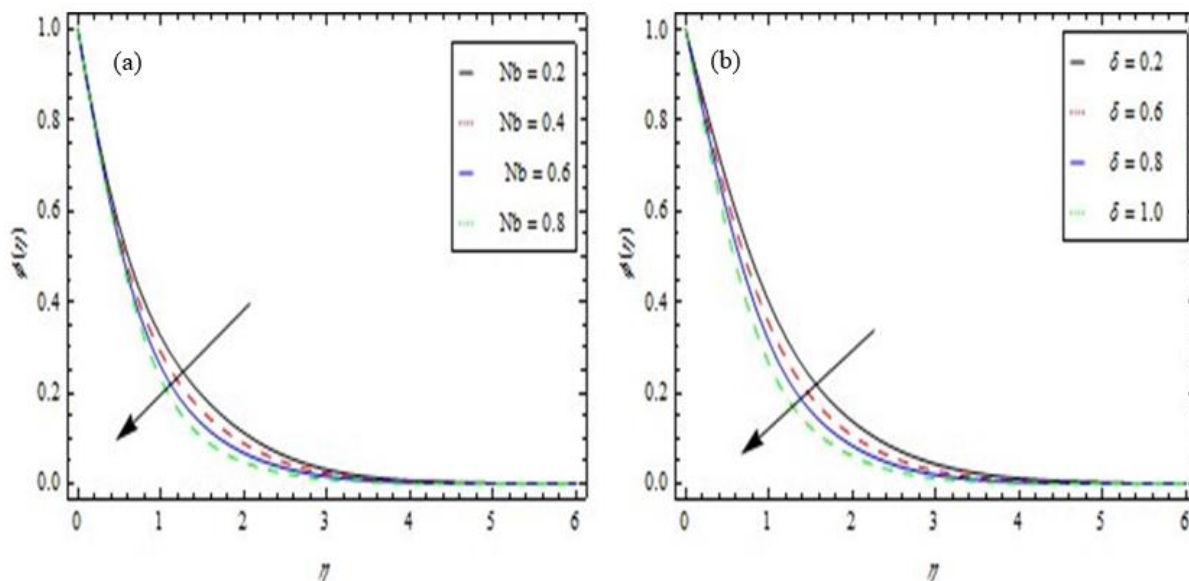**Figure 6.** (a) Influence of S on $\theta(\xi)$, (b) Influence of Sc on $\phi(\xi)$.

c) Concentration profile

Figure 6(b) demonstrates the implications of Schmidt number Sc on concentration. It shows the diffusivity of hydrodynamics divided by mass is the Schmidt number. Furthermore, Sc characterizes the concentration layer's relative thickness to the momentum layer. Mass diffusivity is reduced for a largerSc. Hence, the concentration profile is significantly modified by the presence of Sc in the concentration equation. The graph shows that when Sc values are intensified, the concentration profile decreases. Figure 7(a) shows that when γ increases, the species concentration in the boundary layer decreases, although neither fluid temperature nor speed are affected by an increase in the chemical

reaction parameter γ. The reason for this is the chemical reaction occurring within this system. The main finding is that the extra energy is typically mitigated by the first-order chemical reaction. Thermophoresis can also affect heat transfer processes in the fluid, which can indirectly impact concentration profiles by altering temperature gradients and fluid flow patterns. The thermophoresis parameter influences the strength of the thermophoretic force acting on particles, which can affect their motion and distribution within the fluid. A higher thermophoresis parameter typically implies a stronger thermophoretic force, which improve the thermophoresis parameter Nt and causes the concentration to rise as shown in Figure 7(b). Figure 8(a) illustrates how the concentration distribution changes when the Brownian motion parameter Nb values change. Increased Brownian movements lead to uneven nanoparticle motion, which eventually lowers the concentration of such particles. The Brownian motion parameter directly influences the rate at which particles disperse within the fluid. Higher diffusion coefficients lead to faster spreading of particles away from their initial positions. The influence of the temperature differential parameter δ on the concentration profile is analyzed in Figure 8(b). We determine that the relationship between δ and concentration is inversely proportional. According to the graph, concentration boundary layer thickness condenses when surface and ambient temperatures differ significantly. The effect of the dimensionless activation energy E on the concentration profile is seen in Figure 9(a). The amount of energy required to excite atoms or molecules for a chemical reaction is generally referred to as energy activation. In a chemical process, a significant proportion of atoms should have activation energies that are either less than or equal to translating energy. For rising values of the parameter E, we find that the concentration profile and saline layer thickness increase. We investigate how a higher value for the activation energy parameter E results in a higher term $\exp\left(\frac{-Ea}{KT}\right)$, which varies the concentration profile. For various values of the fitted rate constant n, the concentration dissemination performance is labeled in Figure 9(b). For higher values of n, we find that the component $\gamma(1 + \delta\theta)^n \exp\left(\frac{-E}{1+\delta\theta}\right)$ rises. This component escalates the fluid concentration by destroying the chemical reaction.

**Figure 7.** (a) Influence of γ on $\phi(\xi)$, and (b) influence of Nt on $\phi(\xi)$.

**Figure 8.** (a) Influence of Nb on $\phi(\xi)$, and (b) influence of δ on $\phi(\xi)$.
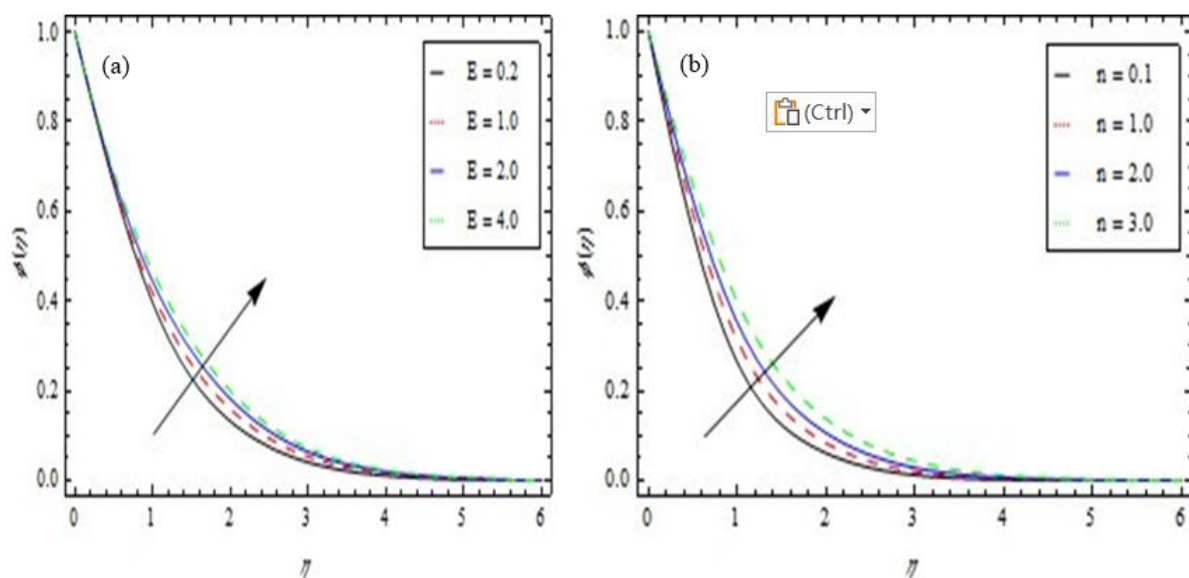
Figure 9. (a) Influence of E on $\phi(\xi)$, and (b) influence of n on $\phi(\xi)$.

The streamline pattern is seen in Figures 10(a) and 10(b). by changing magnetic parameter. The streamlines are more curved near the surface for a less M and less curved near the surface for a higher M. The graphs of isothermal are shown in Figures 11(a) and 11(b). By increasing the values of Prandtl number Pr, the isotherm decreases and rises for lower values of Pr. To investigate the impact of different physical characteristics on coefficient of skin friction, Table 1 has been created. It has been determined that the skin friction coefficient decreases for larger values of the power-law index $\tilde{n}$, Weissenberg number We, mixed convection parameter λ, heat generation parameter S, and Prandtl number Pr, Thermophoresis parameter Nt, and Brownian motion parameter Nb, but increases with the values of the Schmidt number Sc. Table 2 shows the numerical values of the Nusselt number for various physical factors. It is noticed that at larger values of mixed convection parameter λ, Prandtl

number Pr, Thermophoresis parameter Nt, and Brownian motion, parameter Nb, the local Nusselt number rises, while it falls down for larger values of heat generation parameter S and power-law index $\tilde{n}$. The influence of different physical parameters on Sherwood number has been shown numerically by Table 3. Comparison of Nusselt number and Sherwood number by varying activation energy parameters from this study with previously published research [58] is shown in Table 4. Both results are in strong compliance with one another.
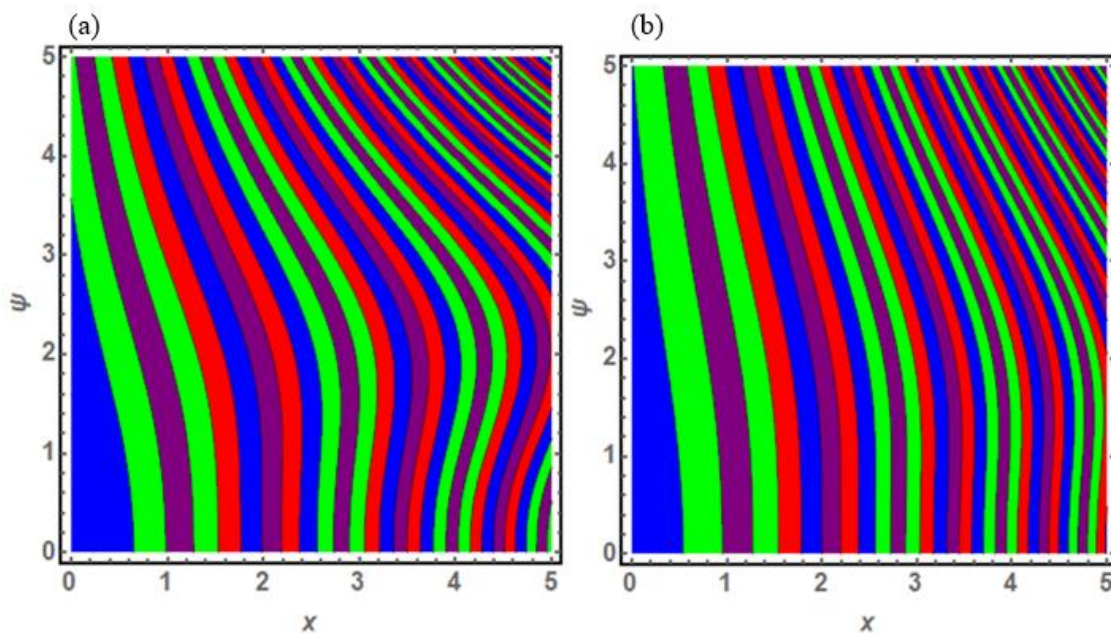
Figure 10. (a) Streamlines when $M = 0.3$, and (b) streamlines when $M = 3.34$.
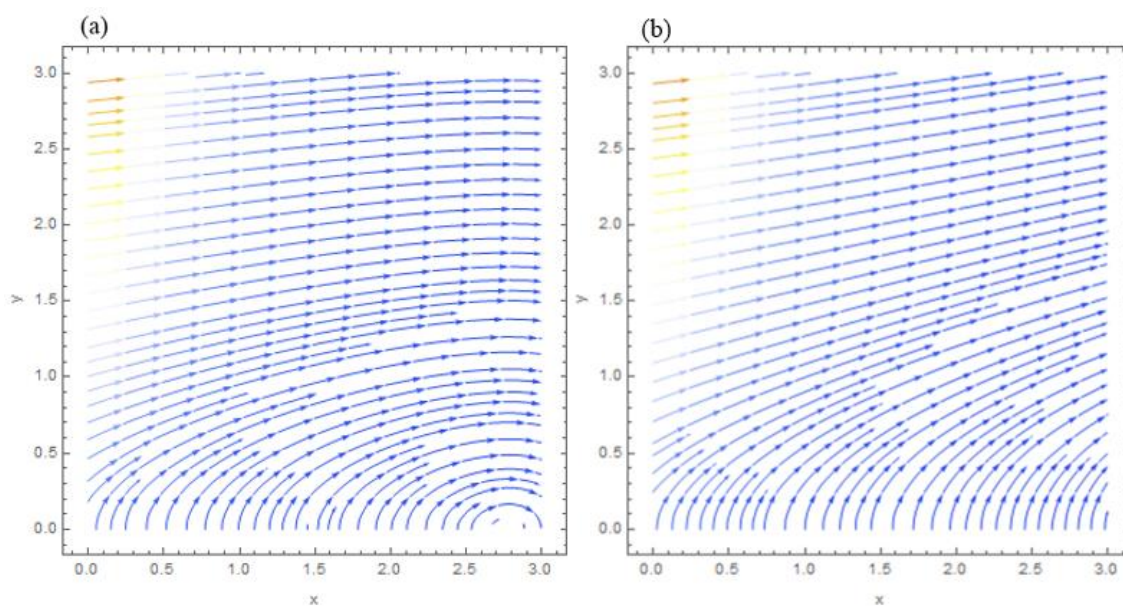
Figure 11. (a) Isothermal graph when $Pr = 0.3$, and (b) isothermal graph when $Pr = 0.6$.

Table 4. Numerical Comparison of $Re_x^{\frac{1}{2}} Nu_x$ and $Re_x^{\frac{1}{2}} Sh_x$ for some physical parameters.

	Nusselt number		Sherwood number	
E	Jawad et al. [58]	Present outcomes	Jawad et al. [58]	Present outcomes
0.1	0.2478	0.24781	0.1652	0.16522
0.2	0.2478	0.24772	0.1652	0.16532
0.3	0.2477	0.24761	0.1652	0.16532

4. Numerical methodology

The nonlinear associated ordinary differential Eqs (7)–(9) along with the given boundary conditions as stated in Eq (10) are numerically solved with the aid of the shooting technique and MATLAB's integrated Bvp4c solver computational tool. This numerical solution is aided by first reducing the higher-order system of equations to a system of first-order differential equations. By substituting the following values, the resulting higher order constraint has been made first order. Let us make an assumption

$$f = f_1, \ f' = f_2, \ f'' = f_3, \ f''' = f_3', \ \theta = f_4, \ \theta' = f_5, \ \theta'' = f_5', \ \phi = f_6, \ \phi' = f_7, \ \phi'' = f_7', f_1' = f_2, \ f_2' = f_3, \tag{13}$$

$$f_3' = \frac{1}{(1-\tilde{n})} [f_2^2 - f_1 f_3 - \tilde{n} We f_3' + M f_2 - \lambda(f_4 + N f_6)], \tag{14}$$

$$f_4' = f_5, \tag{15}$$

$$f_5' = \Pr[f_1 f_5 + Nb f_5 f_7 + Nt f_5^2 + \delta f_4], \tag{16}$$

$$f_6' = f_7, \tag{17}$$

$$f_7' = Sc f_6 - Sc f_1 f_7 - \frac{Nt}{Nb} f_5'. \tag{18}$$

Boundary conditions

$$f_1(0) = 0, \ f_2(\eta) = 1, \ f_5(0) = -\alpha(1 - f_4(0)), \ f_7(0) = -\beta(1 - f_6(0)) = 0, \ f_4(\infty) = 0, \ f_6(\infty) = 0. \tag{19}$$

5. Conclusions

We discuss and examine the mixed convection tangent hyperbolic Nano fluid in a stratified sheet. The governing equations are transformed from PDEs to ODEs while the shooting technique is used. The consequence of dimensionless parameters on velocity, temperature, and concentration profiles is assessed using graphs and tables. The conclusions are as follows:

❖ In tangent hyperbolic nanofluid flow where heat transfer and temperature gradients are present, thermal conductivity and diffusivity coefficients play a crucial role in comprehending and forecasting flow events. Changes in these coefficients can have a major effect on the fluid's thermal behaviour, heat transfer rates, and flow dynamics.

❖ When we increase the magnetic parameter (M), Power law index $(\tilde{n})$ and Weissenberg number (We) tangent hyperbolic nanofluid flow velocity field declines.

❖ Increment in mixed convection (λ) and thermal buoyancy parameter (N), velocity profile $f'(\eta)$

enhancing.

❖ The tangent hyperbolic fluid temperature falls when the Prandtl number (Pr).

❖ The fluid temperature field is improved by increasing the Brownian motion (Nb), thermophoresis (Nt) and heat generation absorption (S) parameter.

❖ With higher values of the Schmidt (Sc), Brownian motion (Nb), and chemical reaction (γ) parameters, the concentration profile is minimal.

❖ An increase in the value of thermophoresis(Nt), temperature difference δ, Energy activation E and rate, the constant n parameter concentration profile also increases.

Author contributions

Reem K. Alhefthi: resources, validation, funding acquisition. Irum Shahzadi: writing-original draft, methodology, formal analysis. Husna A. Khan: writing-original draft, software. Nargis Khan: writing-review and editing, formal analysis, conceptualization. M. S. Hashmi: resources, methodology, software. Mustafa Inc: writing-review and editing, supervision. All authors have read and approved the final version of the manuscript for publication.

Use of AI tools declaration

The authors declare they have not used Artificial Intelligence (AI) tools in the creation of this article.

Acknowledgments

Conflict of interest

The authors declare no conflicts of interest.

References

1. S. U. Choi, J. A. Eastman, *Enhancing thermal conductivity of fluids with nanoparticles*, Illinois: Argonne National Laboratory, 1995.

2. Z. Haddad, H. F. Oztop, E. Abu-Nada, A. Mataoui, A review on natural convective heat transfer of nanofluids, *Renew. Sust. Energy Rev.*, **16** (2012), 5363–5378. http://doi.org/10.1016/j.rser.2012.04.003

3. M. Kalteh, K. Javaherdeh, T. Azarbarzin, Numerical solution of nanofluid mixed convection heat transfer in a lid-driven square cavity with a triangular heat source, *Powder Technol.*, **253** (2014), 780–788. http://doi.org/10.1016/j.powtec.2013.12.039

4. W. F. Sun, The dynamic effect on mechanical contacts between nanoparticles, *Nanoscale*, **5** (2013), 12658–12669. http://doi.org/10.1039/c3nr04354a

5. E. Shahsavani, M. Afrand, R. Kalbasi, Using experimental data to estimate the heat transfer and pressure drop of non-Newtonian nanofluid flow through a circular tube: applicable for use in heat exchangers, *Appl. Therm. Eng.*, **129** (2018), 1573–1581. https://doi.org/10.1016/j.applthermaleng.2017.10.140

6. A. Shafiq, A. B. Çolak, T. N. Sindhu, Designing artificial neural network of nanoparticle diameter and solid–fluid interfacial layer on single-walled carbon nanotubes/ethylene glycol nanofluid flow on thin slendering needles, *Int. J. Numer. Meth. Fl.*, **93** (2021), 3384–3404. https://doi.org/10.1002/fld.5038

7. A. Shafiq, A. B. Çolak, S. A. Lone, T. N. Sindhu, T. Muhammad, Reliability modeling and analysis of mixture of exponential distributions using artificial neural network, *Math. Method. Appl. Sci.*, **47** (2022), 3308–3328. https://doi.org/10.1002/mma.8178

8. A. Shafiq, A. B. Çolak, T. N. Sindhu, Modeling of Soret and Dufour's convective heat transfer in nanofluid flow through a moving needle with artificial neural network, *Arab. J. Sci. Eng.*, **48** (2023), 2807–2820. https://doi.org/10.1007/s13369-022-06945-9

9. A. Shafq, S. A. Lone, T. N. Sindhu, Q. M. Al-Mdallal, G. Rasool, Statistical modeling for bioconvective tangent hyperbolic nanofuid towards stretching surface with zero mass flux condition, *Sci. Rep.*, **11** (2021), 13869. https://doi.org/10.1038/s41598-021-93329-y

10. A. Shafiq, T. N. Sindhu, C. M. Khalique, Numerical investigation and sensitivity analysis on bioconvective tangent hyperbolic nanofluid flow towards stretching surface by response surface methodology, *Alex. Eng. J.*, **59** (2020), 4533–4548. https://doi.org/10.1016/j.aej.2020.08.007

11. A. B. Çolak, A. Shafiq, T. N. Sindhu, Modeling of Darcy-Forchheimer bioconvective Powell Eyring nanofluid with artificial neural network, *Chinese J. Phys.*, **77** (2022), 2435–2453. https://doi.org/10.1016/j.cjph.2022.04.004

12. A. Shafiq, F. Mebarek-Oudina, T. N. Sindhu, A. Abidi, A study of dual stratification on stagnation point Walters' B nanofluid flow via radiative Riga plate a statistical approach, *Eur. Phys. J. Plus*, **136** (2021), 407. https://doi.org/10.1140/epjp/s13360-021-01394-z

13. A. Mishra, M. Kumar, Influence of viscous dissipation and heat generation/absorption on Ag-water nanofluid flow over a Riga plate with suction, *Int. J. Fluid Mech. Res.*, **46** (2019), 113–125. https://doi.org/10.1615/InterJFluidMechRes.2018025291

14. A. Mishra, M. Kumar, Numerical analysis of MHD nanofluid flow over a wedge, including effects of viscous dissipation and heat generation/absorption, using Buongiorno model, *Heat Transf.*, **50** (2021), 8453–8474. https://doi.org/10.1002/htj.22284

15. H. A. Khan, G. Nazeer, S. A. Shehzad, Darcy-Forchheimer tangent hyperbolic nanofluid flow through a vertical cone with non-uniform heat generation, *J. Porous Media*, **26** (2023), 1–14. https://doi.org/10.1615/JPorMedia.2022045225

16. T. Hayat, A. Shafiq, M. Nawaz, A. Alsaedi, MHD axisymmetric flow of third grade fluid between porous disks with heat transfer, *Appl. Math. Mech.*, **33** (2012), 749–764. https://doi.org/10.1007/s10483-012-1584-9

17. T. Hayat, A. Shafiq, A. Alsaedi, M. Awais, MHD axisymmetric flow of third grade fluid between stretching sheets with heat transfer, *Comput. Fluids*, **86** (2013), 103–108. https://doi.org/10.1016/J.compfluid.2013.07.003

18. T. Hayat, A. Shafiq, A. Alsaedi, MHD axisymmetric flow of third grade fluid by a stretching cylinder, *Alex. Eng. J.*, **54** (2015), 205–212. https://doi.org/10.1016/j.aej.2015.03.013

19. A. Shafiq, Z. Hammouch, T. N. Sindhu, Bioconvective MHD flow of tangent hyperbolic nanofluid with newtonian heating, *Int. J. Mech. Sci.*, **133** (2017), 759–766. https://doi.org/10.1016/j.ijmecsci.2017.07.048

20. F. Naseem, A. Shafiq, L. F. Zhao, A. Naseem, MHD biconvective flow of Powell Eyring nanofluid over stretched surface, *AIP Adv.*, **7** (2017), 065013. https://doi.org/10.1063/1.4983014

21. S. Gupta, D. Kumar, J. Singh, MHD mixed convective stagnation point flow and heat transfer of an incompressible nanofluid over an inclined stretching sheet with chemical reaction and radiation, *Int. J. Heat Mass Tran.*, **118** (2018), 378–387. https://doi.org/10.1016/j.ijheatmasstransfer.2017.11.007

22. G. Rasool, T. Zhang, A. J. Chamkha, A. Shafiq, I. Tlili, G. Shahzadi, Entropy generation and consequences of binary chemical reaction on MHD Darcy-Forchheimer Williamson nanofluid flow over non-linearly stretching surface, *Entropy.*, **22** (2020), 18. https://doi.org/10.3390/e22010018

23. A. Mishra, M. Kumar, Ohmic-viscous dissipation and heat generation/absorption effects on MHD nanofluid flow over a stretching cylinder with suction/injection, In: *Advanced computing and communication technologie*, Singapore: Springer, 2019, 45–55. https://doi.org/10.1007/978-981-13-0680-8_5

24. A. Mishra, M. Kumar, Thermal performance of MHD nanofluid flow over a stretching sheet due to viscous dissipation, Joule heating and thermal radiation, *Int. J. Appl. Comput. Math.*, **6** (2020), 123. https://doi.org/10.1007/s40819-020-00869-4

25. A. Mishra, M. Kumar, Velocity and thermal slip effects on MHD nanofluid flow past a stretching cylinder with viscous dissipation and Joule heating, *SN Appl. Sci.*, **2** (2020), 1350. https://doi.org/10.1007/s42452-020-3156-7

26. G. Rasool, A. Shafiq, I. Khan, D. Baleanu, K. S. Nisar, G. Shahzadi, Entropy generation and consequences of MHD in Darcy-Forchheimer nanofluid flow bounded by non-linearly stretching surface, *Symmetry*, **12** (2020), 652. https://doi.org/10.3390/sym12040652

27. A. Shafiq, I. Zari, G. Rasool, I. Tlili, T. S. Khan, On the MHD Casson axisymmetric Marangoni forced convective flow of nanofluids, *Mathematics.*, **7** (2019), 1087. https://doi.org/10.3390/math7111087

28. M. Abbas, N. Khan, M. S. Hashmi, M. Inc, Numerical analysis of Marangoni convective flow of gyrotactic microorganisms in dusty Jeffrey hybrid nanofluid over a Riga plate with Soret and Dufour effects, *J. Therm. Anal. Calorim.*, **148** (2023), 12609–12627. https://doi.org/10.1007/s10973-023-12549-8

29. M. Abbas, N. Khan, M. S. Hashmi, M. Inc, Numerical simulation of magneto thermal Marangoni convective flow of dusty Sutterby hybrid nanofluid with variable thermal conductivity, *ZAMM-Z. Angew. Math. Me.*, **104** (2024), e202300408. https://doi.org/10.1002/zamm.202300408

30. M. Abbas, N. Khan, M. S. Hashmi, H. Alotaibi, H. A. Khan, S. Rezapour, M. Inc, Importance of thermophoretic particles deposition in ternary hybrid nanofluid with local thermal non-equilibrium conditions Hamilton-Crosser and Yamada-Ota models, *Case Stud. Therm. Eng.*, **56** (2024), 104229. https://doi.org/10.1016/j.csite.2024.104229

31. S. Mukhopadhyay, I. C. Mandal, Magnetohydrodynamic (MHD) mixed convection slip flow and heat transfer over a vertical porous plate, *Eng. Sci. Technol.*, **18** (2015), 98–105. https://doi.org/10.1016/j.jestch.2014.10.001

32. M. Imtiaz, T. Hayat, A. Alsaedi, Mixed convection flow of Casson nanofluid over a stretching cylinder with convective boundary conditions, *Adv. Powder Technol.*, **27** (2016), 2245–2256. https://doi.org/10.1016/j.apt.2016.08.011

33. R. U. Haq, Z. Hamouch, S. T. Hussain, T. Mekkaoui, MHD mixed convection flow along a vertically heated sheet, *Int. J. Hydrogen Energ.*, **42** (2017), 15925–15932. https://doi.org/10.1016/j.ijhydene.2017.04.225

34. M. Manzur, M. Khan, M. Rahman, Mixed convection heat transfer to cross fluid with thermal radiation: effects of buoyancy assisting and opposing flows, *Int. J. Mech. Sci.*, **138** (2018), 515–523. https://doi.org/10.1016/j.ijmecsci.2018.02.010

35. K. Hsiao, L. Heat and mass mixed convection for MHD visco-elastic fluid past a stretching sheet with ohmic dissipation, *Commun. Nonlinear Sci.*, **15** (2010), 1803–1812. http://doi.org/10.1016/j.cnsns.2009.07.006

36. M. Waqas, M. Farooq, M. I. Khan, A. Alsaedi, T. Hayat, T. Yasmeen, Magnetohydrodynamic (MHD) mixed convection flow of micropolar liquid due to nonlinear stretched sheet with convective condition, *Int. J. Heat Mass Tran.*, **102** (2016), 766–772. https://doi.org/10.1016/j.ijheatmasstransfer.2016.05.142

37. L. Ali, P. Kumar, Z. Iqbal, S. E. Alhazmi, S. Areekara, M. M. Alqarni, et al., The optimization of heat transfer in thermally convective micropolar-based nanofluid flow by the influence of nanoparticle's diameter and nanolayer via stretching sheet: sensitivity analysis approach, *J. Non-Equil. Thermody.*, **48** (2023), 313–330. https://doi.org/10.1515/jnet-2022-0064

38. Y. I. Seini, O. D. Makinde, MHD boundary layer flow due to exponential stretching surface with radiation and chemical reaction, *Math. Probl. Eng.*, **2013** (2013), 163614. https://doi.org/10.1155/2013/163614

39. S. Sinha, Effect of chemical reaction on an unsteady MHD free convective flow past a porous plate with ramped temperature, *Proceedings of International Conference on Frontier in Mathematics*, 2015, 204–210.

40. L. Ali, B. Ali, T. Iqbal, Finite element analysis of the impact of particles aggregation on the thermal conductivity of nanofluid under chemical reaction, *Wave Random and Complex Media*, **2023** (2023), 2172962. https://doi.org/10.1080/17455030.2023.2172962

41. L. Ali, A. Manan, B. Ali, Maxwell nanofluids: FEM simulation of the effects of suction/injection on the dynamics of rotatory fluid subjected to bioconvection, Lorentz, and Coriolis forces, *Nanomaterials*, **12** (2022), 3453. https://doi.org/10.3390/nano12193453

42. L. Ali, Y. J. Wu, B. Ali, S. Abdal, S. Hussain, The crucial features of aggregation in TiO2-water nanofluid aligned of chemically comprising microorganisms: a FEM approach, *Comput. Math. Appl.*, **123** (2022), 241–251. https://doi.org/10.1016//j.camwa.2022.08.028

43. L. Ali, B. Ali, M. B. Ghori, Melting effect on Cattaneo-Christov and thermal radiation features for aligned MHD nanofluid flow comprising microorganisms to leading edge: FEM approach, *Comput. Math. Appl.*, **109** (2022), 260–269. https://doi.org/10.1016//j.camwa.2022.01.009

44. M. Abbas, N. Khan, M. S. Hashmi, M. Inc, Aspects of chemical reaction and mixed convection in ternary hybrid nanofluid with Marangoni convection and heat source, *Mod. Phys. Lett. B*, **2023** (2023), 2450161. https://doi.org/10.1142/S0217984924501616

45. M. Abbas, N. Khan, S. A. Shehzad, Numerical analysis of Marangoni convected dusty second-grade nanofluid flow in a suspension of chemically reactive microorganisms, *P. I. Mech. Eng. C-J. Mec.*, **238** (2024), 4400–4417. https://doi.org/10.1177//09544062231209828

46. A. R. Bestman, Natural convection boundary layer with suction and mass transfer in a porous medium, *Int. J. Energ. Res.*, **14** (1990), 389–396. https://doi.org/10.1002/er.4440140403

47. O. D. Makinde, P. O. Olanrewaju, W. M. Charles, Unsteady convection with chemical reaction and radiative heat transfer past a flat porous plate moving through a binary mixture, *Afr. Mat.*, **22** (2011), 65–78. https://doi.org/10.1007/s13370-011-0008-z

48. F. E. Alsaadi, I. Ullah, T. Hayat, F. E. Alsaadi, Entropy generation in nonlinear mixed convective flow of nanofluid in porous space influenced by Arrhenius activation energy and thermal radiation, *J. Therm. Anal. Calorim.*, **140** (2020), 799–809. https://doi.org/10.1007/s10973-019-08648-0

49. M. Abbas, N. Khan, A. Alshomrani, M. S. Hashmi, M. Inc, Performance-based comparison of Xue and Yamada–Ota models of ternary hybrid nanofluid flow over a slendering stretching sheet with activation energy and melting phenomena, *Case Stud. Therm. Eng.*, **50** (2023), 103427. https://doi.org/10.1016//j.csite.2023.103427

50. M. Abbas, N. Khan, S. A. Shehzad, Analytical simulation of magneto-marangoni convective flow of Walter-B fluid with activation energy and Soret-Dufour effects, *Adv. Mech. Eng.*, **15 (**2023), 1199049. https://doi.org/10.1177/16878132231199049

51. G. K. Ramesh, A. J. Chamkha, B. J. Gireesha, MHD mixed convection flow of a viscoelastic fluid over a inclined surface with nonuniform heat source/sink, *Can. J. Phys.*, **91**, (2013), 1074–1080. https://doi.org/10.1139/cjp-2013-0173

52. K. L. Hsiao, viscoelastic fluid over a stretching sheet with electromagnetic effects and nonuniform heat source, *Math. Probl. Eng.*, **2010** (2010), 1024–123. https://doi.org/10.1155/2010/740943

53. B. Ramandevi, J. V. R. Reddy, V. Sugunamma, N. Sandeep, Combined influence of viscous dissipation and non-uniform heat source on MHD non-Newtonian fluid flow with Cattaneo-Christov heat flux, *Alex. Eng. J.*, **57** (2018), 1009–1018. https://doi.org/10.1016/j.aej.2017.01.026

54. M. Abbas, N. Khan, M. S. Hashmi, M. Inc, Scrutinization of marangoni convective flow of dusty hybrid nanofluid with gyrotactic microorganisms and thermophoretic particle deposition, *J. Therm. Anal. Calorim.*, **149** (2024), 1443–1463. https://doi.org/10.1007/s10973-023-12750-9

55. M. Bilal, S. Ashbar, Flow and heat transfer analysis of Eyring-Powell fluid over stratified sheet with mixed convection, *J. Egypt. Math. Soc.*, **28** (2020), 40. https://doi.org/10.1186/s42787-020-00103-6

56. K. Muhammad, S. A. M. Abdelmohsen, A. M. M.Abdelbacki, B. Ahmed, Darcy-Forchheimer flow of hybrid nanofluid subject to melting heat: A comparative numerical study via shooting method, *Int. Commun. Heat Mass Tran.*, **135** (2022), 106160. https://doi.org/10.1016/j.icheatmasstransfer.2022.106160

57. H. U. Rasheed, Zeeshan, S. Islam, B. Ali, Q. Shah, R. Ali, Implementation of shooting technique for Buongiorno nanofluid model driven by a continuous permeable surface, *Heat Transf.*, **52** (2023), 3119–3134. https://doi.org/10.1002/htj.22819

58. M. Jawad, A. H. Majeed, K. S. Nisar, M. B. B. Hamida, A. Alasiri, A. M. Hassan, et al., Numerical simulation of chemically reacting Darcy-Forchheimer flow of Buongiorno Maxwell fluid with Arrhenius energy in the appearance of nanoparticles, *Case Stud. Therm. Eng.*, **50** (2023), 103413. https://doi.org/10.1016//j.csite.2023.103413

59. G. K. Ramesh, S. A. Shehzad, T. Hayat, A. Alsaedi, Activation energy and chemical reaction in Maxwell magneto-nanoliquid with passive control of nanoparticle volume fraction, *J. Braz. Soc. Mech. Sci. Eng.*, **40** (2018), 422. https://doi.org/10.1007/s40430-018-1353-8

60. T. Hayat, S. B. Qayyum, B. Ahmad, M. Waqas, Radiative flow of a tangent hyperbolic fluid with convective conditions and chemical reaction, *Eur. Phys. J. Plus*, **131** (2016), 422. https://doi.org/10.1140/epjp/i2016-16422-x